Microscopic evidence of a quantum magnetization process in the $S = \frac{1}{2}$ triangular-lattice Heisenberg-like antiferromagnet $Ba_3CoSb_2O_9$

X. Z. Liu,[1,2] O. Prokhnenko,[1,*] D. Yamamoto,[3] M. Bartkowiak,[1] N. Kurita,[4] and H. Tanaka[4]

[1]*Helmholtz-Zentrum Berlin für Materialien und Energie, Hahn-Meitner-Platz 1, D-14109 Berlin, Germany*

[2]*Songshan Lake Materials Laboratory, Dongguan, Guangdong 523808, China*

[3]*Department of Physics and Mathematics, Aoyama-Gakuin University, Sagamihara, Kanagawa 252-5258, Japan*

[4]*Department of Physics, Tokyo Institute of Technology, Oh-okayama, Meguro-ku Tokyo 152-8551, Japan*

(Received 25 January 2019; revised manuscript received 2 September 2019; published 20 September 2019)

We report results of the neutron scattering investigations of frustrated quantum magnet $Ba_3CoSb_2O_9$ in magnetic fields up to 25.9 T. Contrary to other materials, $Ba_3CoSb_2O_9$ exhibits properties typical of an ideal $S = \frac{1}{2}$ triangular lattice Heisenberg antiferromagnet, making it a perfect model system for testing theoretical predictions. In this work, we looked into the magnetization process in $Ba_3CoSb_2O_9$ on a microscopic scale with a magnetic field applied in plane. A sequence of magnetic phase transitions, including the new high-field phase at 22.5 T reported recently has been followed at low temperatures as a function of field and modeled using the large-size cluster mean-field plus scaling method. Showing good agreement with the model, our results bridge the theory and the experiment providing microscopic information about the high-field spin ordering in $S = \frac{1}{2}$ triangular lattice Heisenberg-like antiferromagnet $Ba_3CoSb_2O_9$.

DOI: 10.1103/PhysRevB.100.094436

I. INTRODUCTION

A frustrated quantum magnet is one of the most interesting subjects in condensed matter physics. A $S = \frac{1}{2}$ triangular lattice Heisenberg antiferromagnet (TLHAF) is its typical example, where the combined geometrical spin frustration and quantum fluctuations result in intriguing quantum phenomena for both the ground state [1–8] and magnetic excitations [9–13]. At zero field TLHAF orders in a so-called 120° or Y spin configuration below the Neél temperature [14–20]. Despite that, its ground state in the presence of a magnetic field, H, cannot be determined uniquely based on the classical model, as it will be infinitely degenerate [14,15]. In the quantum $S = \frac{1}{2}$ limit, the ground state in a magnetic field is determined by the energy of quantum fluctuations [1,3] which stabilizes an up-up-down (UUD) spin state in finite magnetic fields [1–8]. Corresponding magnetization curves with plateaus at one-third of the saturation magnetization, M_s, have been observed in some representative systems, such as Cs_2CuBr_4 [4,21], $Ba_3CoSb_2O_9$ [22], $CsCuCl_3$ [23], $Ba_2La_2CoTe_2O_{12}$ [24], as well as $S = 1$ system $Ba_3NiSb_2O_9$ [25].

In this work, we focus on the magnetic-field-induced quantum phases in the hexagonal $Ba_3CoSb_2O_9$ compound, which closely approximates a paradigmatic $S = \frac{1}{2}$ TLHAF system as the effective magnetic moment of Co^{2+} in an octahedral environment can be described by a pseudo $S = \frac{1}{2}$ at temperatures below 50 K [22,26]. The compound has the highly symmetric $P6_3/mmc$ space group with a uniform triangular lattice of Co^{2+} ions [27]. A weak easy-plane anisotropy has been obtained by fitting ESR measurements with a semiclassical torque-equation analysis [28], while a recent theoretical calculation predicted a 20% easy-plane anisotropy [29] and inelastic neutron scattering (INS) experiments revealed a 10% difference of the exchange parameters between the in-plane and out-of-plane directions [30]. Although a non-negligible anisotropy may exist, the system exhibits a close-to-ideal TLHAF behavior. In zero-field $Ba_3CoSb_2O_9$ orders in a 120° spin structure in the ab plane below $T_N = 3.8$ K [27,30] as visualized in Fig. 1(a), and displays a $\frac{1}{3}M_s$ plateau in magnetic fields [22,28,31]. Thus $Ba_3CoSb_2O_9$ can be viewed as a model system of an ideal TLHAF for testing theoretical predictions.

In this respect, it is interesting to look into the field dependence of the spin state of $Ba_3CoSb_2O_9$ in the entire field range up to saturation. The ground state in magnetic field has been investigated by a number of techniques including magnetization [22,28], ESR [28], sound velocity [32], and NMR [33] measurements. The results can be summarized as follows. For the magnetic fields H parallel to the ab plane, a $\frac{1}{3}M_s$ magnetization plateau corresponding to an UUD spin configuration [Fig. 1(b)] is observed in the field range for $0.30H_s < H < 0.47H_s$ with the saturation field of $H_s = 31.9$ T, which is in good agreement with the theoretical calculations [5–8]. The dynamical properties of the $\frac{1}{3}M_s$ plateau phase have been reported recently using a combination of nonlinear spin-wave theory and INS measurements [34]. For $0.47H_s < H < H_s$, the system is expected to order in the so-called 0-planar or V phase as shown in Fig. 1(c) in the case of the pure two-dimensional model. However, recently, a new first-order field-induced phase transition was observed at about $0.7H_s$ around $\frac{3}{5}M_s$ [28]. This transition is manifested by an anomaly in the magnetic susceptibility and a strong spin-lattice relaxation observed by NMR [28,33]. A number of hypotheses were put forward to explain these anomalies as a result of a phase transition between different co-planar

*Corresponding author: prokhnenko@helmholtz-berlin.de

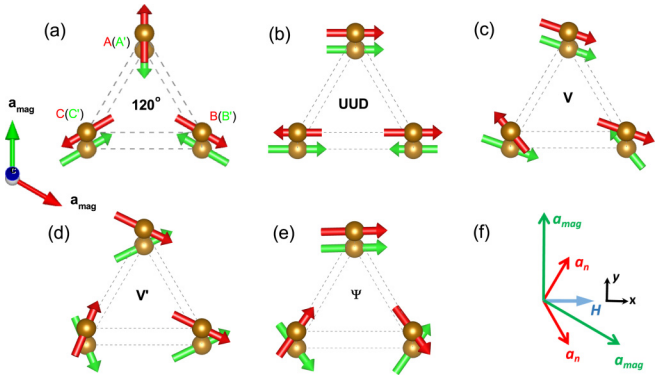

FIG. 1. [(a)–(e)] Spins in a magnetic unit cell (view along the c-axis) of the calculated $Ba_3CoSb_2O_9$ spin configurations in magnetic fields applied along the reciprocal $\mathbf{a}^*_{\rm mag}$ direction. The magnetic unit cell is defined as $\sqrt{3}a_n \times \sqrt{3}a_n \times c$ and its relation with the crystallographic one is shown in (f) [27]. Green- (sites A, B, C) and red-colored (sites A', B', C') spins correspond to adjacent layers along the c axis. (a) and (b) show the zero field 120° structure and the UUD structure ($0.3H_s < H < 0.47H_s$). (c)–(e) display the co-planar V phase ($0.47H_s < H < 0.7H_s$) and the proposed high-field co-planar V' and Ψ phases ($0.7H_s < H < H_s$). (f) shows the crystallographic and magnetic unit cells as well as the field direction and the Cartesian coordinate system applied in the theoretical calculations.

states (between the V and Ψ or V and V' states as shown in Figs. 1(c)–1(e) [28,29,33], as an effect of nonmagnetic impurities [35] or the spins aligning along the field-transverse direction on one of the sublattices [36]. Finally, above H_s the system becomes fully polarized. The saturation field along the *c-axis* is very close to the in-plane value, reflecting a weak anisotropy [28].

Although the agreement between experiment (bulk magnetization) and theory in low fields is good, up-to-date there is neither direct confirmation of the spin configurations in high fields nor their field evolution. It becomes especially crucial now when the new high-field anomaly is observed in bulk measurements. The main experimental challenge here is that the saturation field in $Ba_3CoSb_2O_9$ is very high, $H_s = 31.9$ T, making the transitions at $0.47H_s = 15$ and $0.7H_s = 22.4$ T not accessible by standard means such as neutron scattering. In this paper we report a direct observation of high-field phases in $Ba_3CoSb_2O_9$ using HFM/EXED - high-field facility for neutron scattering at BER II research reactor at Helmholtz-Zentrum Berlin (HZB) [37]. The unique combination of the high-field magnet (HFM) and the dedicated time-of-flight Extreme Environment Diffractometer (EXED) enables neutron scattering experiments in continuous magnetic fields up to 25.9 T and temperatures down to ∼1 K. Reported measurements allow us to conclude that the anomaly at $0.7H_s$ represents a real phase transition. Supported by by theoretical modeling using the large-size cluster mean-field plus scaling (CMF + S) method [29,38,39], they point to the transition between coplanar V and V' phases, where the latter is a result of a weak but finite antiferromagnetic interlayer interaction [29]. More generally, our experimental data in extreme conditions provide a critical test of the existing theories and their capabilities to reproduce physical properties of real materials with great level of detail.

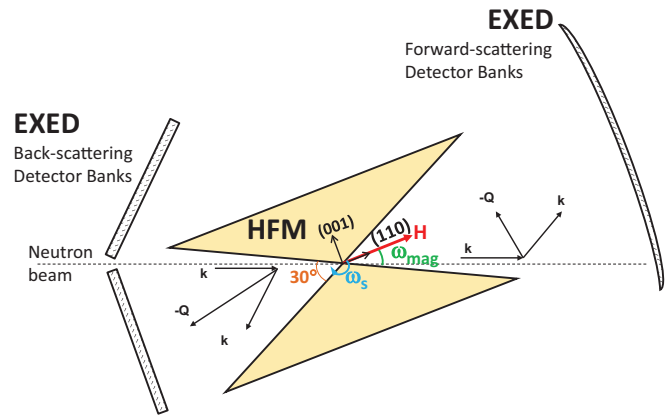

FIG. 2. Schematic presentation (top view) of the high-field scattering setup. The picture includes the HFM and the EXED detectors, sample orientation and scattering geometry for the forward- and back-scattering detectors displayed for a single wavelength (wave vector **k**).

II. EXPERIMENTAL

$Ba_3CoSb_2O_9$ single crystal with a size of $4 \times 4 \times 4$ mm^3 and weight of 0.42 g was grown from the melts, using a Pt crucible. For details of sample preparation, see Ref. [40]. The high-field neutron measurements have been performed at the HFM/EXED high-field neutron facility at the BER-II research reactor at Helmholtz-Zentrum Berlin [37]. The facility consists of a hybrid solenoid (horizontal) High-Field Magnet (HFM) and a dedicated time-of-flight Extreme Environment Diffractometer (EXED) [41,42]. The magnet has 30° conical openings on both ends and can be rotated with respect to the incident neutron beam by an angle $\omega_{\rm mag} \leqslant 12°$. Combined with the TOF technique, it enables a reasonable reciprocal space coverage in the forward- and backscattering directions where position-sensitive detectors are placed. The scattering setup is sketched in Fig. 2. The sample was placed in a He-flow cryostat inserted into the room temperature bore of the magnet. This cryostat is equipped with a rotation stage around the vertical axis, $\omega_s \approx 180°$, allowing to increase the accessible reciprocal space significantly in the case of zero field measurements. All the high-field measurements were performed with a fixed ω_s (i.e., fixed direction of magnetic field with respect to the sample). The sample has been aligned with the $[h, h, 0]$ direction along the field and $[0, 0, l]$ lying in the horizontal plane perpendicular to the field. A sketch of the scattering geometry is shown as an inset in Fig. 4(b). All measurements were performed at the base temperature, value of which is given in Fig. 4.

III. NEUTRON DIFFRACTION

A. Zero-field measurements

Previous sample characterization has been reported in a number of publications, see Refs. [28,40]. On EXED, the crystal structure of $Ba_3CoSb_2O_9$ at 1.5 K was verified using a set of ten nuclear reflections accessible in the forward scattering detector bank. To bring these peaks into the accessible range,the sample was rotated around the vertical axis and the data were collected at a fixed magnet rotation angle with a

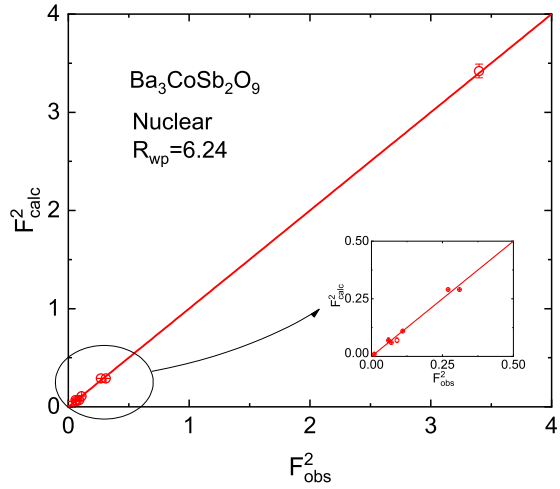

FIG. 3. Refinement of the nuclear structure of $Ba_3CoSb_2O_9$ at 1.5 K: calculated vs observed intensities for the collected nuclear peaks as obtained using FULLPROF. The straight line shows $F^2_{obs} = F^2_{calc}$. The insert displays low F^2_{obs} part of the plot.

wavelength band of 0.7–7 Å. The results of the refinement performed using the FULLPROF suite software package [43] are displayed in Fig. 3. They clearly demonstrate that the crystal structure does not change upon cooling.

In addition to the nuclear reflections, two groups of equivalent magnetic peaks with $l = -1$ and -3 could be accessed at 1.5 K. They can be indexed using propagation vector $(\frac{1}{3}, \frac{1}{3}, 1)$ in agreement with literature [27,30]. Averaging the equivalent peaks, we refined the magnetic structure using a 120° coplanar model. The obtained magnetic moment amounts to 1.292(1) μ_B which is in good agreement with the experimentally derived value [27].

B. High-field measurements

Application of a horizontal magnetic field, which has to be kept parallel to a given crystallographic direction, significantly restricts the accessible reciprocal space in the experiment. With $H \parallel [h, h, 0]$ with precision of 1°, $(0, 0, l)$-type reflections with $l = -1, -2$ could be accessed. In order to measure magnetic satellites, the sample has been rotated around the vertical axis by $\omega_s = 12°$ towards the c axis giving access to the nuclear $(-1, 1, -2)$ reflection and two equivalent magnetic satellites $(\frac{1}{3}, -\frac{2}{3}, -3)$ and $(-\frac{2}{3}, \frac{1}{3}, -3)$. With such an angular offset, a finite field component along the c axis, $H_\perp$, becomes inevitable. At the maximum field of 25.9 T, $H_\perp$ is about 5.4 T which is well below the transition field (∼10 T) to the co-planar state along the c axis. All field values given hereafter refer to the in-plane component, H_{ab}.

First of all, we look into field dependence of nuclear reflections $(0, 0, -2)$ and $(-1, 1, -2)$ which is visualized in Figs. 4(a) and 4(b), respectively. Both curves display only the magnetic contribution after the nuclear one has been subtracted. For $(0, 0, -2)$ two datasets measured in different experiments are displayed. One set covers a larger field range while the other represents a detailed scan performed around $0.7H_s$ (=22.4 T) where the anomaly in bulk measurements have been observed. At zero field, the spin configuration is symmetric 120° in-plane order. In this case $(0, 0, -2)$ and $(-1, 1, -2)$ reflections contain only the structural contribution. Upon application of a magnetic field, a monotonously increasing magnetic contribution is observed reflecting a ferromagnetic component induced in the sample. As neutrons are sensitive to the component of the magnetic moment perpendicular to the momentum transfer, the magnetic contribution to $(0, 0, -2)$ should be directly proportional to the square of the in-plane magnetization, M. Dashed line in Fig. 4(a) denotes the M^2 multiplied by a scale factor. The magnetization data are taken from Ref. [28]. One can see an excellent agreement over the whole field range. The low field part

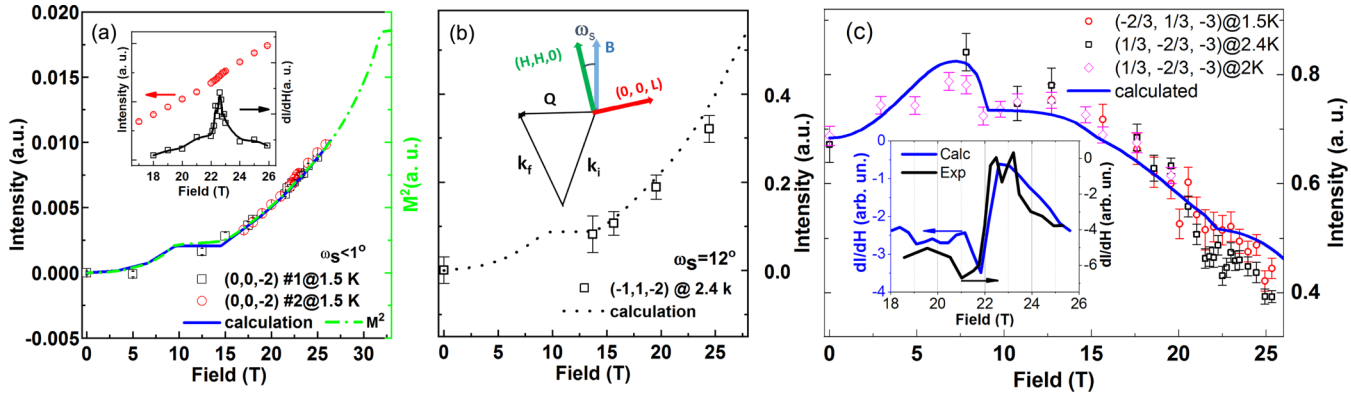

FIG. 4. Measured (square and circle symbols) and calculated (solid lines) magnetic intensities as a function of magnetic field for the transitions between the 120°, UUD, V, and V' phases. (a) The magnetic contribution to the intensity of $(0, 0, -2)$ as a function of field. Two experimental datasets (1 and 2) are shown. The theoretical calculation (solid blue) and square of magnetization (dashed green, refer to right axis) are also presented. The inset displays the dataset 2 and its first derivative across the phase transition at 22.5 T. (b) Experimental and theoretical curves of the magnetic contribution to $(-1, 1, -2)$ as a function of field. The inset shows a sketch of the experiment geometry. (c) The field dependence of the intensity of the $(\frac{1}{3}, -\frac{2}{3}, -3)$ and $(-\frac{2}{3}, \frac{1}{3}, -3)$ reflections. The inset visualizes a first derivative of the averaged experimental and theoretical datasets across the phase transition at 22.5 T. For all the datasets, the results have been scaled by a constant to allow the comparison between the experiment and the theory.

has less data points since there is no ambiguity in the zero-field and plateau structures [27,30,34], and magnetization measurements probe the same signal. However, the most interesting field range around the transition at 22.4 T is covered in detail. Here, the scan (2) with fine field steps shows an anomaly as displayed in the inset of Fig. 4(a). To better visualize the anomaly, the first derivative of intensity vs. field is also presented in the same figure. A peak appearing around 22.5 T is clearly observed and consistent with the magnetization data [28]. The $(-1,\ 1,\ -2)$ reflection displayed in Fig. 4(b) has been measured as a reference for the antiferromagnetic reflections described below. As a result, the data have been collected only at a small number of fields. It precludes a detailed comparison with the model in the entire field range. However, the measured data points overlap with the expected theoretical curve quite well.

The nuclear $(0,\ 0,\ l)$ reflections with l being odd are not allowed in the given space group. However, the accessible reflection with $l = -1$ has been checked as it provides information about the transverse components of spin configurations in high field. Indeed, for all the considered co-planar phases such as V, V', and Ψ structures, a finite magnetic $(0,\ 0,\ -1)$ reflection would correspond to an uncompensated transverse component perpendicular to the field. Thus $(0,\ 0,\ -1)$ is indicative of the transverse moment magnitude. To examine this issue, long measurements at fields 20 and 25 T, i.e., below and above the transition at 22.5 T, have been performed (not shown). At each field the counting time was more than 10 times longer than for $(0,\ 0,\ -2)$ reflection. Since no visible reflection was detected within the statistical error, we can conclude that the transverse components of the three sublattices cancel out in the phases below and above 22.5 T.

Now, we turn to the purely magnetic $(\frac{1}{3}, -\frac{2}{3}, -3)$ and $(-\frac{2}{3}, \frac{1}{3}, -3)$ reflections, the field dependence of which is displayed in Fig. 4(c). Due to the weak intensities of the reflections, a background measured at 10 K (i.e., well above $T_N = 3.8\ K$) has been subtracted to get only the magnetic signal. In contrast to the nuclear $(0,\ 0,\ -2)$ and $(-1,\ 1,\ -2)$ reflections, which both increase with field, the behavior of the magnetic reflections is more complex. Three characteristic regions can be seen when inspecting the curves. The first one is characterized by an increase in intensity at fields up to ~9.5 T corresponding to the 120° structure and its modification in field. The second one is a plateau around 9.5–15 T corresponding to the UUD structure. Finally, there is a shoulder-like anomaly around ~22.5 T. The first derivative of the intensity changes in a jump-like manner across this transition as is depicted in the inset of Fig. 4(c). This anomaly in both the raw data and its derivative is very clear and easily detectable as compared to the subtle change in intensity of $(0,\ 0,\ -2)$ visualized in Fig. 4(a).

IV. THEORETICAL CALCULATIONS

The above results unambiguously indicate that the anomaly at 22.5 T is a result of a magnetic phase transition. Thus, the effect of magnetic impurities or the spins aligning along the field-transverse direction on one of the sublattices can be excluded [35,36]. The next question which arises is: what are the spin configurations below and above the transition?

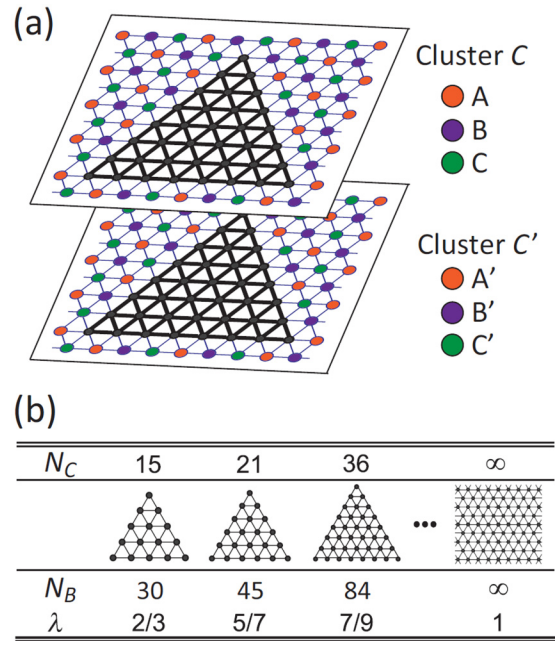

FIG. 5. (a) Cluster of $N_C = 36$ spins embedded in neighboring two layers with the six-sublattice structure. (b) List of the clusters used in the CMF + S analysis with scaling parameter λ.

As the reciprocal space coverage in the high-field experiment is rather limited, and the number of observed magnetic reflections does not allow to perform a proper refinement of the magnetic structures, we carried out extensive theoretical calculations to model the experimental results and explain the observed behavior. The calculations were done with the CMF + S method for the following $S = \frac{1}{2}$ XXZ model on stacked weakly coupled triangular layers [29,38,39]:

$$\hat{\mathcal{H}} = \sum_{\langle i,j\rangle}\left[J\left(\hat{S}_i^x\hat{S}_j^x + \hat{S}_i^y\hat{S}_j^y\right) + J_z\hat{S}_i^z\hat{S}_j^z\right] + J'\sum_{\langle i,l\rangle'}\hat{\boldsymbol{S}}_i\cdot\hat{\boldsymbol{S}}_l - \boldsymbol{H}\cdot\sum_i\hat{\boldsymbol{S}}_i \quad (1)$$

with the intralayer (J, J_z) and interlayer (J') nearest-neighbor couplings. For comparison with experiment, we use $J_z/J = 0.8$ and $J'/J = 0.05$ on the assumption that $Ba_3CoSb_2O_9$ has the easy-plane anisotropy of about 15%–20 %, according to the latest theoretical estimations [34,39]. In addition, the calculations with $J_z/J = 0.9$ have been performed (not shown) but the neutron data are not sensitive enough to detect the difference between the models with $J_z/J = 0.8$ and 0.9.

In order to solve the cluster problem [29], in this work we extended the maximum cluster size up to $N_C = 36$ sites by applying the density matrix renormalization group (DMRG) method [44], and finally performed extrapolation to the infinite clusters' number. The triangular-shaped clusters employed here are listed in in Fig. 5. The interaction between a cluster-edge spin and its neighboring spin at an out-of-cluster site with sublattice index μ is replaced by an effective magnetic field $(J/m_\mu^x, J/m_\mu^y, J_z/m_\mu^z)$ acting on the edge spin. Under the $3 \times 2 = 6$ sublattice ansatz ($\mu = A, B, C, A', B', C'$), we calculate the sublattice magnetic moments $\boldsymbol{m}_\mu$ by solving

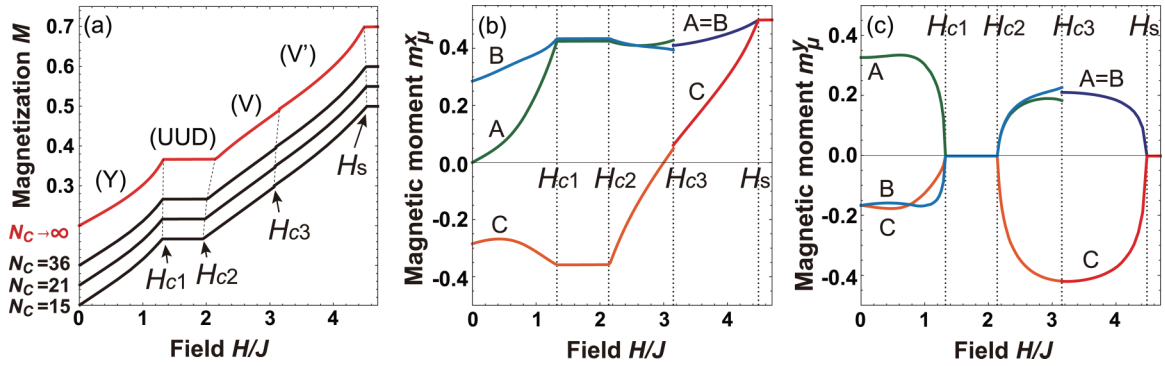

FIG. 6. (a) Theoretically simulated ground-state magnetization curves for $N_C = 15$, 21, 36, and ∞ (from bottom to top) when $H \parallel ab$. The curves apart from the bottom one are vertically shifted by 0.05, 0.1, and 0.2, respectively, for clarity. [(b) and (c)] Sublattice magnetic moments $\boldsymbol{m}_\mu$ ($\mu = A, B, C$) calculated by CMF + S ($\lambda \to 1$) when $H \parallel ab$. The field-perpendicular components m^z_μ are zero. The values of $\boldsymbol{m}_\mu$ for $\mu = A', B', C'$ are obtained through the relations with A, B, C as displayed in Fig. 1.

the set of six self-consistent equations

$$\boldsymbol{m}_\mu = \frac{3}{N_C} \sum_{\langle i_\mu \rangle} \langle \hat{\boldsymbol{S}}_{i_\mu} \rangle \ (\mu = A, B, C, A', B', C'). \tag{2}$$

Here, the sum $\sum_{\langle i_\mu \rangle}$ runs over all μ sites within the cluster embedded in a layer with A, B, C (A', B', C') sublattices for $\mu = A, B, C$ ($\mu = A', B', C'$). The ground-state expectation values $\langle \hat{\boldsymbol{S}}_{i_\mu} \rangle$ with respect to the cluster Hamiltonian $\hat{\mathcal{H}}_C$ (or $\hat{\mathcal{H}}_{C'}$) are obtained by solving equivalent one-dimensional problems with long-range interactions and effective mean fields by means of DMRG [44]. Note that both $\hat{\mathcal{H}}_C$ and $\hat{\mathcal{H}}_{C'}$ are functions of all the sublattice magnetic moments $\boldsymbol{m}_\mu$ in a self-consistent way via effective mean fields. The dimension of the truncated matrix product states in DMRG is taken to be sufficiently large for a good convergence of $\boldsymbol{m}_\mu$ (within $\lesssim 10^{-8}$).

For comparison with the nuclear $(0, 0, -2)$ reflection, we calculate the theoretical magnetization curve $M(H) = (m^x_A + m^x_B + m^x_C + m^x_{A'} + m^x_{B'} + m^x_{C'})/6$ with setting $\boldsymbol{H} = (H, 0, 0)_{\rm mag}$, where the xyz coordinate system is defined with respect to the magnetic unit cell, $\sqrt{3}a \times \sqrt{3}a \times c$, as follows: $x \parallel H$, $z \parallel c$ and $y \perp x \perp z$ [Fig. 1(f)]. In this case, due to the easy-plane anisotropy, the magnetic moments $\boldsymbol{m}_\mu$ lie in the xy plane with the coplanar or collinear configurations depicted in Fig. 1. Figure 6(a) shows $M(H)$ obtained for $N_C = 15, 21, 36$ and its extrapolation to $N_C \to \infty (\lambda \to 1)$ with $\lambda = N_B/(3N_C)$. Here, N_B is the number of bonds within the cluster. One clearly sees all the anomalies at H_{c1}, H_{c2}, and H_{c3} observed in the magnetization and neutron diffraction, see Fig. 4. The extrapolated values of the transition fields are $H_{c1} = 0.295H_s$, $H_{c2} = 0.476H_s$, and $H_{c3} = 0.720H_s$, respectively, with the saturation field $H_s = 4.49J$. Each component of the sublattice magnetic moments at $\lambda \to 1$ is shown in Figs. 6(b) and 6(c). Different moment sizes per site reflect both the true quantum nature of these transitions and presence of the interlayer antiferromagnetic coupling.

As for the magnetic $(\frac{1}{3}, -\frac{2}{3}, -3)$ and $(-\frac{2}{3}, \frac{1}{3}, -3)$ reflections we set $\boldsymbol{H} = (H \cos\omega_s, 0, H \sin\omega_s)$ with $\omega_s = 12^\circ$ reflecting the experimental settings. Although the sublattice moments $\boldsymbol{m}_\mu$ no longer lie in the xy plane due to a small but finite component of the magnetic field perpendicular to the triangular plane, $H \sin\omega_s$, the magnetic order is only slightly deformed from the exact coplanar or collinear configurations displayed in Fig. 1. In this case, the extrapolated values of the transition fields are $H_{c1} = 0.295H_s$, $H_{c2} = 0.497H_s$, and $H_{c3} = 0.720H_s$, respectively, with the saturation field $H_s = 4.46J$ [Fig. 7(a)]. Each calculated component of the sublattice magnetic moments for the infinite cluster size is shown in Figs. 7(b)–7(d). It is worth noting the presence of a finite z component because of a 12° field offset.

V. DISCUSSION

Using the theoretically derived values of the magnetic moments and their orientation with respect to the crystallographic axis, the magnetic structure factors for all zero- and expected high-field phases have been simulated using FULLPROF

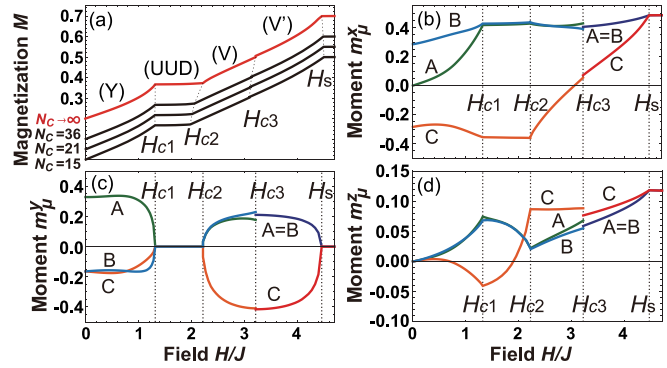

FIG. 7. Theoretical calculations for the field $H \sim 12^\circ$ off [1,1,0] towards [0,0,1] for the transitions between the 120°, UUD, V, and V' phases. (a) Calculated ground-state magnetization curves for $N_C = 15$, 21, 36, and ∞ (from bottom to top). The curves apart from the bottom one are vertically shifted for clarity by 0.05, 0.1, and 0.2, respectively. [(b)–(d)] Sublattice magnetic moments $\boldsymbol{m}_\mu$ ($\mu = A, B, C$) calculated by CMF + S ($\lambda \to 1$). The values of $\boldsymbol{m}_\mu$ for $\mu = A', B', C'$ are obtained through the relations with A, B, C displayed in Figs. 1(a)–1(e) while the coordinate system is depicted in Fig. 1(f).

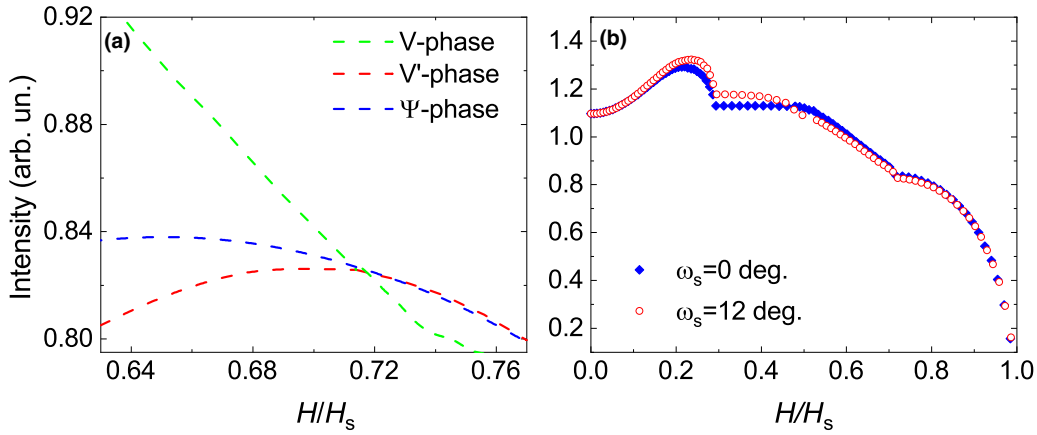

FIG. 8. Integrated intensities of the magnetic $(\frac{1}{3}, -\frac{2}{3}, -3)$ and $(-\frac{2}{3}, \frac{1}{3}, -3)$ reflections (a) calculated for the V, V', and Ψ phases across the H_{c3} transition and (b) calculated for $\omega_s = 0^\circ$ and 12° in the entire field range.

[43]. The neutron-scattering cross section is related to the components of ordered magnetic moments $\boldsymbol{m}_\mu$ as follows [45]:

$$\frac{d\sigma}{d\Omega} = \frac{1}{N_m}\frac{2\pi^3}{v_0}\sum_{\tau_i}\delta(\boldsymbol{Q}-\boldsymbol{\tau}_i)|\hat{\boldsymbol{Q}}\times\hat{\boldsymbol{F}}_M(\boldsymbol{\tau}_i)\times\hat{\boldsymbol{Q}}|^2, \quad (3)$$

where

$$\hat{\boldsymbol{F}}_M(\boldsymbol{Q}) = \gamma r_0 \sum_\mu f_\mu(\boldsymbol{Q})\langle\boldsymbol{m}_\mu\rangle e^{i\boldsymbol{Q}\cdot\boldsymbol{r}_\mu}e^{-W_\mu(\boldsymbol{Q})} \quad (4)$$

in which $\gamma = 1.9132$, $r_0 = e^2/(m_e c^2) = 2.8179 \times 10^{-15}$ m is the classical radius of the electron. N_m is the number of magnetic ions in each magnetic unit cell, v_0 is the volume of magnetic cell, $\boldsymbol{\tau}_i$ denotes the magnetic propagation vectors, μ is the position of the magnetic atom within a magnetic cell, $f_\mu(\boldsymbol{Q})$ is the atomic form factor of Co^{2+}, $\langle\boldsymbol{m}_\mu\rangle = (m_x, m_y, m_z)_\mu$ describes the magnetic moment vector, $\hat{\boldsymbol{Q}}$ is a unit vector along $\boldsymbol{Q}$ direction, and W_j is Debye-Waller factor.

The resulting magnetic intensities in comparison with the measured ones are presented as solid lines in Figs. 4(a)–4(c). Note that the ground-state magnetic configurations given in Fig. 1 are degenerate with respect to the π rotation around the field direction. Those equivalent degenerate states give different contributions to the scattering intensity in the case of the direction of $\boldsymbol{Q}$ breaking the symmetry. The theoretical curves of the scattering intensity shown in the Fig. 2(c) are averaged over those different contributions under the assumption that the spin configurations connected by the π rotation around the field direction are represented by equally populated domains in the compound.

The overall agreement between the theoretical calculations and experiment is very good. First, the (0, 0, −2) reflection shows a plateau reflecting the UUD phase in agreement with the experiment. However, from the (0, 0, −2) reflection alone, one cannot distinguish whether V, V', or Ψ structure is the ground state below H_{c3} as all curves would look identical above the UUD phase up to saturation. Still, if there is a transition it should be of the first order between the V and V' phases, as observed in the experiment [see Fig. 4(a) and insert therein], and of the second order between the V and Ψ structures. The most interesting case is the field dependence of the intensities of purely magnetic $(\frac{1}{3}, -\frac{2}{3}, -3)$ and $(-\frac{2}{3}, \frac{1}{3}, -3)$ reflections as displayed in Fig. 4(c). One sees that the theory reproduces all features of the experimental curves quite well. Some deviation between experimental and theoretical data, especially at higher fields, we attribute to finite temperature effects as discussed below. At low fields the intensities increase, reflecting the modification of the 120° structure by the field [Figs. 7(b)–7(d)]. Around 10 T they drop and remain constant up to 15 T, as expected for the UUD structure. Above 15 T, the intensities start decreasing linearly, indicating that the system underwent a transition to the V state. The most important result, however, is that the V-V' transition indeed appears as a shoulderlike anomaly in the theoretical calculations. Its specific shape is a result of the intersection of the linearly decreasing magnetic intensity in the V phase with its parabolic dependence in the V' phase. Inspecting the field dependence of the first derivative shown as an inset in Fig. 4(c), one finds a good quantitative agreement with the experiment. One has to note that there is some ambiguity between the V' and Ψ structures as they are indistinguishable by neutron diffraction. Closer look at the behavior of the V, V', and Ψ phases across the H_{c3} is given in Fig. 8(a). However, in combination with the neutron data on the (0, 0, −2) reflection, and the theory implying that the Ψ phase may only be realized for $J' > 0.25J$ [29,33], we are led to conclude that the ground state structure above H_{c3} is V'.

Finally, we looked into possible reasons of some deviation between experimental and theoretical data visible especially at higher fields [see Fig. 4(c)]. Figure 8(b) displays the results of CMF + S calculations made for the sample oriented along [1, 1, 0] ($\omega_s = 0^\circ$) and 12° off towards [0,0,1] direction ($\omega_s = 12^\circ$). These data shows robustness of our modeling results with respect to sample misalignment. Although some smearing effects are seen in the vicinity of the 120°-UUD and UUD-V transitions, there is very little effect on the high-field V-V' transition. We note that 12° misalignment is about an order of magnitude larger than that one might have had in the experiment. The fact that our zero field magnetic structure is in good agreement with that reported by other groups [27,30] led us to exclude disorder or oxygen deficiency related effects in this particular sample. Thus we believe that

finite temperature effects could be a plausible reason for the observed discrepancy.

VI. CONCLUSION

In conclusion, we have examined the ground-state spin configurations of $Ba_3CoSb_2O_9$ in magnetic fields up to 25.9 T using neutron scattering technique supported by theoretical CMF + S calculations. The overall agreement between the theory and the experiment gives for the first time a direct evidence of a microscopic magnetization process in the TL-HAF model system $Ba_3CoSb_2O_9$. The UUD magnetic order at $\frac{1}{3}M_s$ as well as a recently discovered transition at around $\frac{3}{5}M_s$ were observed by anomalies in magnetic intensities as a function of field, and confirmed by the calculations. Our observations disclose the microscopic nature of the transition of $Ba_3CoSb_2O_9$ at around $0.7H_s$, which has been found by magnetization measurements and proposed by the theory, and provides a deeper insight into the physics of $S = \frac{1}{2}$ triangular lattice Heisenberg antiferromagnets.

ACKNOWLEDGMENTS

We greatly acknowledge R. Wahle, S. Gerischer, S. Kempfer, and P. Heller for their support at the HFM/EXED facility at the Helmholtz-Zentrum Berlin. D.Y. is supported by KAKENHI from Japan Society for the Promotion of Science, Grants No. 17H02926 and No. 18K03525, and CREST from Japan Science and Technology Agency No. JPMJCR1673. H.T. and N.K. are supported by Grants-in-Aid for Scientific Research (A) (No. 17H01142) and (C) (No. 16K05414) from Japan Society for the Promotion of Science, respectively.

[1] H. Nishimori and S. Miyashita, J. Phys. Soc. Jpn. **55**, 4448 (1986).
[2] T. Nikuni and H. Shiba, J. Phys. Soc. Jpn. **62**, 3268 (1993).
[3] A. V. Chubukov and D. I. Golosov, J. Phys.: Condens. Matter **3**, 69 (1991).
[4] J. Alicea, A. V. Chubukov, and O. A. Starykh, Phys. Rev. Lett. **102**, 137201 (2009).
[5] D. J. J. Farnell, R. Zinke, J. Schulenburg, and J. Richter, J. Phys.: Condens. Matter **21**, 406002 (2009).
[6] A. Honecker, J. Phys.: Condens. Matter **11**, 4697 (1999).
[7] T. Sakai and H. Nakano, Phys. Rev. B **83**, 100405(R) (2011).
[8] C. Hotta, S. Nishimoto, and N. Shibata, Phys. Rev. B **87**, 115128 (2013).
[9] O. A. Starykh, A. V. Chubukov, and A. G. Abanov, Phys. Rev. B **74**, 180403(R) (2006).
[10] A. L. Chernyshev and M. E. Zhitomirsky, Phys. Rev. B **79**, 144416 (2009).
[11] M. Mourigal, W. T. Fuhrman, A. L. Chernyshev, and M. E. Zhitomirsky, Phys. Rev. B **88**, 094407 (2013).
[12] E. A. Ghioldi, A. Mezio, L. O. Manuel, R. R. P. Singh, J. Oitmaa, and A. E. Trumper, Phys. Rev. B **91**, 134423 (2015).
[13] E. A. Ghioldi, M. G. Gonzalez, S.-S. Zhang, Y. Kamiya, L. O. Manuel, A. E. Trumper, and C. D. Batista, Phys. Rev. B **98**, 184403 (2018).
[14] D. A. Huse and V. Elser, Phys. Rev. Lett. **60**, 2531 (1988).
[15] T. Jolicoeur and J. C. Le Guillou, Phys. Rev. B **40**, 2727 (1989).
[16] B. Bernu, P. Lecheminant, C. Lhuillier, and L. Pierre, Phys. Rev. B **50**, 10048 (1994).
[17] R. R. P. Singh and D. A. Huse, Phys. Rev. Lett. **68**, 1766 (1992).
[18] L. Capriotti, A. E. Trumper, and S. Sorella, Phys. Rev. Lett. **82**, 3899 (1999).
[19] W. H. Zheng, J. O. Fjærestad, R. R. P. Singh, R. H. McKenzie, and R. Coldea, Phys. Rev. B **74**, 224420 (2006).
[20] S. R. White and A. L. Chernyshev, Phys. Rev. Lett. **99**, 127004 (2007).
[21] T. Ono, H. Tanaka, H. Aruga Katori, F. Ishikawa, H. Mitamura, and T. Goto, Phys. Rev. B **67**, 104431 (2003).
[22] Y. Shirata, H. Tanaka, A. Matsuo, and K. Kindo, Phys. Rev. Lett. **108**, 057205 (2012).
[23] A. Sera, Y. Kousaka, J. Akimitsu, M. Sera, and K. Inoue, Phys. Rev. B **96**, 014419 (2017).
[24] Y. Kojima, M. Watanabe, N. Kurita, H. Tanaka, A. Matsuo, K. Kindo, and M. Avdeev, Phys. Rev. B **98**, 174406 (2018).
[25] Y. Shirata, H. Tanaka, T. Ono, A. Matsuo, K. Kindo, and H. Nakano, J. Phys. Soc. Jpn. **80**, 093702 (2011).
[26] M. E. Lines, Phys. Rev. **131**, 546 (1963).
[27] Y. Doi, Y. Hinatsu, and K. Ohoyama, J. Phys.: Condens. Matter **16**, 8923 (2004).
[28] T. Susuki, N. Kurita, T. Tanaka, H. Nojiri, A. Matsuo, K. Kindo, and H. Tanaka, Phys. Rev. Lett. **110**, 267201 (2013).
[29] D. Yamamoto, G. Marmorini, and I. Danshita, Phys. Rev. Lett. **114**, 027201 (2015).
[30] J. Ma, Y. Kamiya, T. Hong, H. B. Cao, G. Ehlers, W. Tian, C. D. Batista, Z. L. Dun, H. D. Zhou, and M. Matsuda, Phys. Rev. Lett. **116**, 087201 (2016).
[31] H. D. Zhou, C. Xu, A. M. Hallas, H. J. Silverstein, C. R. Wiebe, I. Umegaki, J. Q. Yan, T. P. Murphy, J.-H. Park, Y. Qiu, J. R. D. Copley, J. S. Gardner, and Y. Takano, Phys. Rev. Lett. **109**, 267206 (2012).
[32] G. Quirion, M. Lapointe-Major, M. Poirier, J. A. Quilliam, Z. L. Dun, and H. D. Zhou, Phys. Rev. B **92**, 014414 (2015).
[33] G. Koutroulakis, T. Zhou, Y. Kamiya, J. D. Thompson, H. D. Zhou, C. D. Batista, and S. E. Brown, Phys. Rev. B **91**, 024410 (2015).
[34] Y. Kamiya, L. Ge, T. Hong, Y. Qiu, D. L. Quintero-Castro, Z. Lu, H. B. Cao, M. Matsuda, E. S. Choi, C. D. Batista, M. Mourigal, H. D. Zhou, and J. Ma, Nat. Commun. **9**, 2666 (2018).
[35] V. S. Maryasin and M. E. Zhitomirsky, Phys. Rev. Lett. **111**, 247201 (2013)
[36] D. Sellmann, X. F. Zhang, and S. Eggert, Phys. Rev. B **91**, 081104(R) (2015)
[37] O. Prokhnenko, P. Smeibidl, W.-D. Stein, M. Bartkowiak, and N. Stüsser, J. Large Scale Research Facilities JLSRF **3**, A115 (2017).
[38] D. Yamamoto, A. Masaki, and I. Danshita, Phys. Rev. B **86**, 054516 (2012).

[39] D. Yamamoto, G. Marmorini, and I. Danshita, Phys. Rev. Lett. **112**, 127203 (2014).

[40] S. Ito, N. Kurita, H. Tanaka, S. Ohira-Kawamura, K. Nakajima, S. Itoh, K. Kuwahara, and K. Kakurai, Nat. Commun. **8**, 235 (2017).

[41] P. Smeibidl, M. Bird, H. Ehmler, I. Dixon, J. Heinrich, M. Hoffmann, S. Kempfer, S. Bole, J. Toth, O. Prokhnenko, and B. Lake, IEEE Trans. Appl. Supercond. **26**, 1 (2016).

[42] O. Prokhnenko, W. Stein, H. Bleif, M. Fromme, M. Bartkowiak, and T. Wilpert, Rev. Sci. Instrum. **86**, 033102 (2015).

[43] J. Rodríguez-Carvajal, Physica B **192**, 55 (1993).

[44] D. Yamamoto, G. Marmorini, M. Tabata, K. Sakakura, and I. Danshita, arXiv:1808.08916.

[45] *Neutron Scattering from Magnetic Materials*, edited by T. Chatterji (Elsevier, 2006).